Available online at www.sciencedirect.com
ScienceDirect
International Journal of Multiphase Flow 33 (2007) 1296–1307
International Journal of Multiphase Flow
www.elsevier.com/locate/ijmulflow

Experimental study on the condensation of supersonic steam jet submerged in quiescent subcooled water: Steam plume shape and heat transfer

Xin-Zhuang Wu, Jun-Jie Yan *, Shu-Feng Shao, Yan Cao, Ji-Ping Liu

State Key Laboratory of Multiphase Flow in Power Engineering, Xi'an Jiaotong University, Xi'an 710049, PR China

Received 24 January 2007; received in revised form 23 May 2007

Abstract

The condensation of supersonic steam jet submerged in the quiescent subcooled water was investigated experimentally. The results indicated that the shape of steam plume was controlled by the steam exit pressure and water temperature. Six different shapes of steam plume were observed under the present test conditions. Their distribution as a function of the steam exit pressures and water temperatures was given. As the steam mass velocity and water temperature increase, the measured maximum expansion ratio and dimensionless penetration length of steam plume were in the ranges of 1.08–1.95 and 3.05–13.15, respectively. The average heat transfer coefficient of supersonic steam jet condensation was found to be in the range of 0.63–3.44 MW/m^2K. An analytical model of steam plume was found and the correlations to predict the maximum expansion ratio, dimensionless penetration length and average heat transfer coefficient were also investigated.

Keywords: Condensation; Heat transfer; Interface; Steam jet; Supersonic

1. Introduction

The phenomena of steam-water direct contact condensation has been investigated extensively for its importance in many industrial operations, such as underwater propulsion system, direct contact heat exchanger, chemical mixing equipment, steam jet driven injector and nuclear reactor safety system. When the steam was injected into the quiescent subcooled water, several condensation modes including chugging, bubbling and jet would appear according to the thermal hydraulic conditions (Liang and Griffith, 1994). The steam

* Corresponding author. Tel./fax: +86 29 8266 5741.
E-mail address: yanjj@mail.xjtu.edu.cn (J.-J. Yan).

0301-9322/$ - see front matter © 2007 Elsevier Ltd. All rights reserved.
doi:10.1016/j.ijmultiphaseflow.2007.06.004

jet condensation can be divided into three modes according to the steam velocity at nozzle exit, i.e. subsonic jet, sonic jet and supersonic jet.

The condensation of subsonic or sonic steam jet submerged in the quiescent subcooled water has been studied by many researchers. Kerney et al. (1972) and Weimer et al. (1973) studied the penetration length of sonic steam jet submerged horizontally in quiescent subcooled water experimentally and theoretically, the correlations to calculate the dimensionless penetration length was also given. Simpson and Chan (1982) experimentally investigated the hydrodynamics of subsonic steam jet vertically downwards into the subcooled water. The average heat transfer coefficient for subsonic jets in their experiment was about one-tenth to one-fifth of sonic jet values. The mechanism of the condensation process of subsonic steam jet vertically upwards into water was reported by Kostyuk (1985), the results indicated that the geometry of the contacting zone of phases was governed by the magnitude of the temperature head. Chen and Faeth (1982) considered the turbulent condensing vapor jets submerged in subcooled liquids, a model was presented for numerical simulation assuming an idealiazed plume shape and a homogeneous two phase flow. The pressure and temperature in the surrounding zone inside a steam jet condensing in a subcooled water pool were measured by Giovanni et al. (1984), an adopted model to describe the phenomena was introduced. Takeuchi et al. (1994) discussed the process of steam jet into a subcooled water in AP600 core makeup tank, a numerical method was established to simulate the process. Chan and Lee (1982) described a regime map for low steam mass flux (less than 200 kg/m^2s) of direct contact condensation. Chun et al. (1996) gave a qualitative regime map for high steam mass flux (more than 200 kg/m^2s). They found that the average heat transfer coefficient of sonic steam jet condensation was in the range of 1.0–3.5 MW/m^2K, which mainly depended on the steam mass flux. Eden et al. (1998) explored the centerline pressure and cavity shape of horizontal plane choked vapor jets with low condensation potential, the results were compared with the case of air jets.

Recently, the condensation of steam jet applied in the nuclear reactor was studied experimentally and theoretically by several Korea researchers (Seong et al., 2000; Kim et al., 2001; Youn et al., 2003; Kim and Song, 2003; Kim et al., 2004). The numerical method of this process was given by Kazuyuki et al. (2002), Petrovic (2005) and Sagar et al. (2006). The summary of previous experimental work is given in Table 1, which shows that the direct contact condensation of steam jet submerged in the subcooled water was investigated by many researchers. However, there is almost no experiment about the condensation of supersonic steam jet except three groups of data by Kerney et al. (1972). The supersonic steam jet has been used in the industrial operation, such as steam jet driven injector. Maybe it will be used in the design of the nuclear reactor safety system or other operations. By far, the experimental data about this process is very limited. In the present wok, the plume shape of supersonic steam jet submerged in the subcooled water was experimentally studied and the correlations to predict the maximum expansion ratio, penetration length and heat transfer coefficient were also investigated.

2. Experimental system

The experimental system is shown in Fig. 1, which mainly consists of a steam generator, a surge tank, a water vessel of 630 mm × 630 mm × 1500 mm and associated valves. The steam generator with capability of 10 kW supplied continuously the steam with a quality very close to 1. The upper part of the water vessel was open to the ambient with an overflow, the two observation windows with the same size were designed for observation and taking pictures. The steam was injected into the subcooled water through a nozzle which was fixed on the wall of water vessel by a flange. The nozzle was made of stainless steel with an adiabatic coat to prevent the occurrence of condensation along the inner surface. The scheme of the nozzle is also shown in Fig. 1. In present work, two nozzles (a and b) with convergent- divergent inner passage were tested for the research on the condensation of supersonic steam jet. The experimental conditions are shown in Table 2.

The steam flow rate was measured by a vortex type steam flowmeter (accuracy 0.5%FS). The pressure and temperature in the jet exit were measured by a mobile probe, which was equipped with a pitot or a K-type thermocouple. The pitot was connected with two pressure transducers (MSI, accuracy 0.1%FS). The water temperature in water vessel was measured by four K-type thermocouples. A high-speed video camera was used to take pictures of steam plume. All signals were processed by the data acquisition system consisting of PC and A/D converter.

Table 1
List of previous experimental investigations on the condensation of steam jet submerged in water

Researchers	Nozzle position/type/diameter	Flow condition	Experimental conditions	Research methods	Main conclusions
Kerney et al. (1972)	Horizontal; (a) flat head, $d_0 = 0.4$–9.5 mm; (b) conical, $d_0 = 1.58$, 6.35 mm; (c) convergent–divergent, $d_0 = 10.1$,11.2 mm	Sonic; maybe supersonic for nozzle (c)	Atmospheric pressure, $T_w = 301$–358 K, $G_0 = 332$–2050 kg/(m^{2}s)	Visual observation and experimental measurement	Steam plume penetration length $l/d_0 = 0.26B^{-1}(G_0/G_m)^{0.5}$
Weimer et al. (1973)	Horizontal; convergent nozzle, $d_0 = 3.17$ mm	Sonic	Changing pressure, $T_w = 297$–356 K, $G_0 = 332$–2050 kg/(m^{2}s)	Experimental measurement and theoretical derivation	Steam plume penetration length $l/d_0 = 17.75B^{-1}(\rho_\infty/\rho_s)^{-0.5}(G_0/G_m)^{0.5}$
Simpson and Chan (1982)	Vertically downward; straight pipe, $d_0 = 6.35$, 15.9, 22.2 mm	Subsonic	Atmospheric pressure, $T_w = 298$–338 K, $G_0 = 147.2$–333.3 kg/(m^{2}s)	Visual observation and experimental measurement	Three basic interfacial motions: bubble growth, bubble translation and bubble separation. The average heat transfer coefficient for subsonic jets is about one-fifth to one-tenth of sonic jet values
Chan and Lee (1982)	Vertically downward; straight pipe, $d_0 = 2$, 4, 6 mm	Subsonic, sonic	Atmospheric pressure, $T_w = 313$–363 K, $G_0 = 1$–175 kg/(m^{2}s)	Visual observation and experimental measurement	A regime map for direct contact condensation was developed including three main modes: steam chugging, oscillatory bubble and oscillatory jet
Giovanni et al. (1984)	Vertically downward; straight pipe, $d_0 = 2$, 4, 6 mm	Sonic	Atmospheric pressure, $T_w = 293$–348 K, $G_0 = 200$–800 kg/(m^{2}s)	Visual observation, experimental measurement and theoretical derivation	Steam plume penetration length: $l/d_0 = 0.5a^{-1}\psi_1^{-1}$; half jet width: $db/dx = 0.22$; axial temperature: $T_{ax} = 9.31d_0(\rho_v/\rho_l)^{0.5}[L_v + c_p(T_{sat} - T_w)]/[2c_p(x + b_1/0.22–1)]$
Kostyuk (1985)	Vertically upward; straight pipe, $d_0 = 4$, 10 mm	Subsonic	Atmospheric pressure, $T_w = 288$–353 K, $u_0 = 53$–400 m/s	Visual observation and experimental measurement	The condensation is oscillating and the zone geometry of phases contact is governed by magnitude of the temperature
Chun et al. (1996)	Horizontal; straight pipe, $d_0 = 1.35$, 4.45, 7.65, 10.85 mm	Sonic	Atmospheric pressure, $T_w = 289$–360 K, $G_0 = 200$–1500 kg/(m^{2}s)	Visual observation and experimental measurement	Condensation regime map was divided into six regions in detail. Expansion ratio: 1.0–2.3; steam plume penetration length: $l/d_0 = 0.5923B^{-0.66}(G_0/G_m)^{0.3444}$; heat transfer coefficient: $h = 1.3583c_pG_mB^{0.0405}(G_0/G_m)^{0.3714}$
Eden et al. (1998)	Horizontal; plane nozzle, slot height: 3 mm, width: 36 mm	Sonic	Atmospheric pressure, $B = 8.1$–161, $m_0 = 0.064$–0.113 kg/s	Visual observation, experimental measurement and numerical simulation	The shock cell structure was seen and the degree of pressure recovery substantially less than comparable submerged air jet, which was attributed to the combined effects of condensation of vapor and evaporation of bath liquid
Kim et al. (2001)	Horizontal; straight pipe, $d_0 = 5$, 7.1, 10.15, 15.5, 20 mm	Sonic	Atmospheric pressure, $T_w = 308$–353 K, $G_0 = 250$–1188 kg/(m^{2}s)	Visual observation, experimental measurement	Expansion ratio: 1.05–2.3; steam plume penetration length: $l/d_0 = 0.503B^{-0.70127}(G_0/G_m)^{0.47688}$; heat transfer coefficient: $h = 1.4453c_pG_mB^{0.03587}(G_0/G_m)^{0.13315}$
Youn et al. (2003)	Horizontal; straight pipe, $d_0 = 5/8$, 6/8 in.	Subsonic	Atmospheric pressure, $T_w = 308$–353 K, $G_0 = 10$–80 kg/(m^{2}s)	Visual observation, experimental measurement	The condensation is in the chugging region and the high pressure pulses were generated with relatively low frequency which was little affected by the water temperature. A critical value of steam mass flux was found where the pressure pulses generation rate increased suddenly

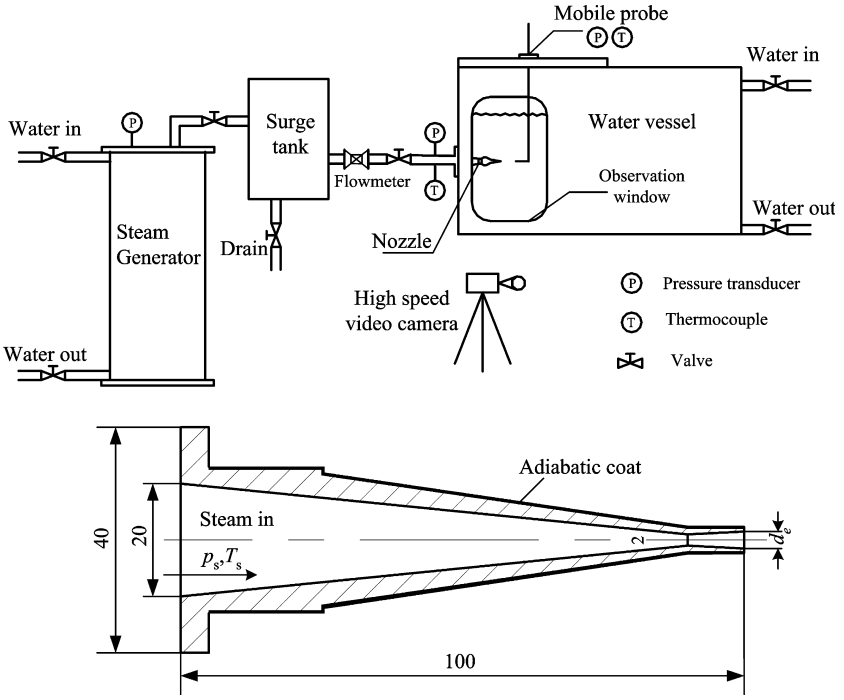

Fig. 1. Schematic diagram of experimental system and nozzle.

Table 2
Test conditions in experiment

Parameters	Value
Steam inlet pressure p_s, MPa	0.20–0.50
Steam mass flux at nozzle throat G_{cr}, kg/m^2 s	298–723
Water temperature T_w, K	293–343
Ambient pressure p_a, MPa	0.099
Throat diameter of nozzle d_{th}, mm	2.0
Exit diameter of nozzle a, and b d_e, mm	2.2 and 3.0
Submerged depth of nozzle exit H_{sub}, mm	200

3. Experimental results and correlations

3.1. Regions and process of the jet flow and condensation

Fig. 2 shows the analytical model of the jet flow and condensation. When the steam was injected into the subcooled water, the direct contact condensation occurred. When the flow and condensation reached the equilibrium, there were three regions existing in the flow field. The first region consisting of the pure steam was called steam plume. The second region was called steam-water two-phase mixing region, where the water closing to the saturation temperature at the interface mixed with small steam bubbles. In the mixing region, both phases were in turbulent motion with eddies due to the momentum or kinetic energy carried by the condensing steam and the velocity of water (Sagar et al., 2006). The interface between the first two regions was the phase interface, along which the convective heat and mass transfer occurred. Beyond the phase interface was the third region: the single-phase water at certain temperature and pressure.

At the case of stable jet flow and condensation, a stable steam plume was obtained for the steady condensation rate which was equal to the steam mass flux at the nozzle exit. Under the interaction of both phases, a

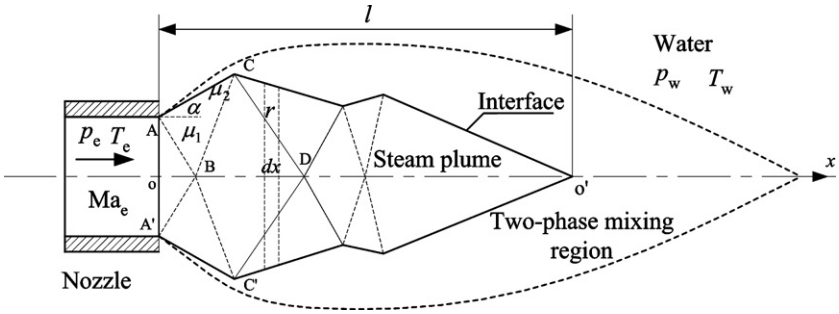

Fig. 2. Analytical model of the jet flow and condensation.

"channel" consisting of the incompressible water formed, where the compressible steam flowed at high velocity and condensed at the wall of the "channel" until completely condensed. Consequently, the different shapes of steam plume would form under different conditions of steam and water.

3.2. Shape of steam plume

In previous experiments of sonic steam jet, the two typical shapes of steam plume were observed. The first shape called conical shape by Giovanni et al. (1984), Chun et al. (1996) and Kim et al. (2001) is shown in Fig. 3 (Shape A), and the second shape called ellipsoidal shape by Chun et al. (1996) and Kim et al. (2001) is shown in Fig. 3 (Shape B). In this paper, Fig. 3 shows the six different shapes of steam plume of supersonic jet condensation, the shapes were typically observed under different test conditions. According to the experimental results and the thermodynamic analysis, the shape of steam plume was controlled by the steam exit pressure and the water temperature in water vessel. For the over-expanded steam jet case (the steam exit pressure was smaller than the pressure of water surrounding the nozzle exit), the shock wave may appear at nozzle exit because of supersonic flow (the Mach number at nozzle exit was 2.09). After the shock wave, the steam plume would be constricted at low water temperature (Shape A in Fig. 3). With increasing water temperature, the expansion and compression of steam plume would arise after the shock wave (Shape E and F in Fig. 3). In contrast, for the under-expanded steam jet case (the steam exit pressure was larger than the pressure of water surrounding the nozzle exit), the expansion wave may occur at nozzle exit due to supersonic flow (the Mach

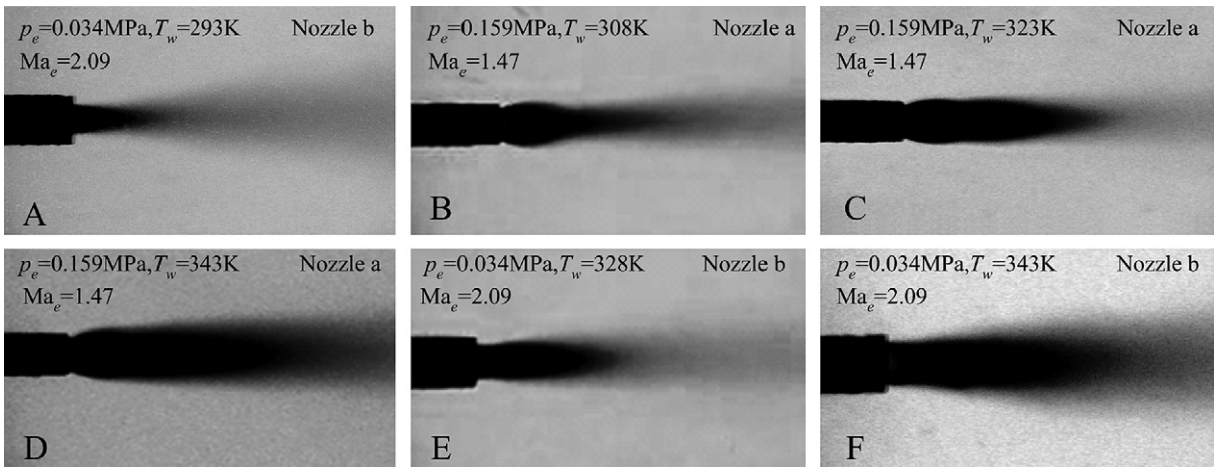

Fig. 3. Shapes of steam plume under different test conditions (Supersonic jet condensation, $d_e = 2.2$, 3.0 mm).

number at nozzle exit was 1.47), the shapes of steam plume were shown in Fig. 3 (Shape B, C and D in Fig. 3). According to the view point of supersonic compressible flow, for under-expanded case, the expansion wave would occur and reflect periodically. For over-expanded case, the shock wave would occur and reflect periodically. But for steam jet, the expansion and shock wave would disappear gradually due to the condensation. The shape C in Fig. 3 shows two periods of expansion wave. The shape E is not contractive directly, but after a reflection. The two examples indicated that the expansion and contraction may occur periodically if there was no mass, momentum and energy transfer with the surrounding water. The number of expansion or compression was determined by the condensation capacity of the surrounding water, which mainly depends on its temperature. With increasing water temperature, the shape of one expansion (Shape B in Fig. 3) and shape of double expansions (Shape C in Fig. 3) appeared orderly. When the water temperature was further increased (higher than 343 K), the interface of steam-water two phases would become oscillating, and the steam plume would become emanative (Shape D and F in Fig. 3). The distribution of steam plume shape under different steam exit pressures and water temperatures is shown in Fig. 4.

3.3. Maximum expansion ratio of steam plume

For the case of under-expanded steam jet, the steam will expand, a maximum expansion ratio of steam plume exists (ratio between the maximum diameter of steam plume and the diameter of nozzle exit). Obviously, the maximum expansion ratio must be obtained at the place of the first expansion because of the transfer and interaction between the two phases.

Fig. 5 shows the maximum expansion ratio under different experimental conditions (G_{cr} is the steam mass flux at nozzle throat). With increasing steam mass flux and water temperature, the maximum expansion ratio of steam plume increases, the values are in the range of 1.08–1.95, as shown in Table 3. The upper limit of the maximum expansion ratio in this work is smaller than those of Chun et al. (1996) and Kim et al. (2001). The possible reason is that the maximum steam mass flux in present study is smaller than those of previous studies.

Neglecting entrainment, frictional effect and heat transfer in the region from the nozzle exit to the place of the first expansion, according to the theory of one-dimensional steady isentropic flow, the following relation can be obtained (Currie, 2003).

$$\frac{p_1}{p_e} = \left(\frac{2+(\gamma-1)Ma_e^2}{2+(\gamma-1)Ma_1^2}\right)^{\gamma/(\gamma-1)} \tag{1}$$

where p_e, Ma_e are the pressure and Mach number at the nozzle exit, p_1, Ma_1 are the pressure and Mach number after the first expansion wave ABA' (as shown in Fig. 2), γ is the isentropic exponent.

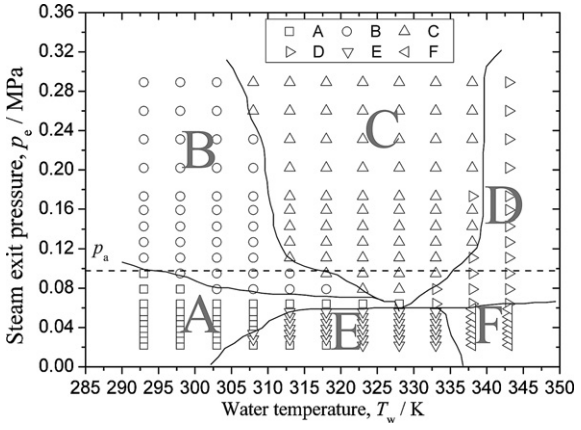

Fig. 4. Distribution of steam plume shape under different steam exit pressures and water temperatures.

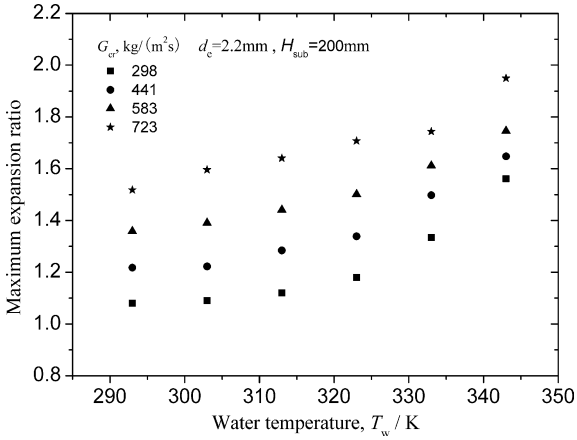

Fig. 5. Maximum expansion ratio of steam plume under different test conditions.

Table 3
Contrast of maximum expansion ratio

Researchers	Steam mass flux (kg/m^{2}s)	Maximum expansion ratio
Chun et al. (1996)	200–1500	1.00–2.3
Kim et al. (2001)	250–1188	1.05–2.3
Present work	298–723	1.08–1.95

The patulous angle of steam flow α after the expansion wave ABA' is

$$\alpha = \left(\frac{\gamma+1}{\gamma-1}\right)^{1/2}\{\arctan[(\gamma-1)(Ma_1^2-1)/(\gamma+1)]^{1/2} - \arctan[(\gamma-1)(Ma_e^2-1)/(\gamma+1)]^{1/2}\} - [\arctan(Ma_1^2-1)^{1/2} - \arctan(Ma_e^2-1)^{1/2}] \quad (2)$$

The expansion angle of the expansion wave (angle between the direction of steam flow before the wave and that of the wave) can be calculated by

$$\mu = \arcsin(1/Ma) \quad (3)$$

Then according to the geometrical relations in Fig. 2, the expansion ratio of steam plume at the place of the first expansion can be obtained.

$$R_{ex} = \frac{\sin(\alpha+\mu_1)\sin(\alpha+\mu_2)}{\sin\mu_1 \sin\mu_2} \quad (4)$$

Considering the effect of water temperature on the maximum expansion ratio, the following relation was given to predict the maximum expansion ratio.

$$R_{ex}^{max} = k\frac{\sin(\alpha+\mu_1)\sin(\alpha+\mu_2)}{\sin\mu_1 \sin\mu_2} \quad (5)$$

where k is the correctional coefficient depending on the water temperature T_w, $k = T_w/273$.

The predicted expansion ratio by Eq. (5) compared with the experimental expansion ratio are shown in Fig. 6, which indicates that the maximum predicted errors is 24.4%.

3.4. Penetration length of steam plume

As shown in Fig. 2, the penetration length of steam plume OO' is defined as the axial distance of pure steam. For the case of stable sonic steam jet condensation, this length has been investigated by many researchers (Kerney et al., 1972; Weimer et al., 1973; Chen and Faeth, 1982; Giovanni et al., 1984; Chun et al., 1996;

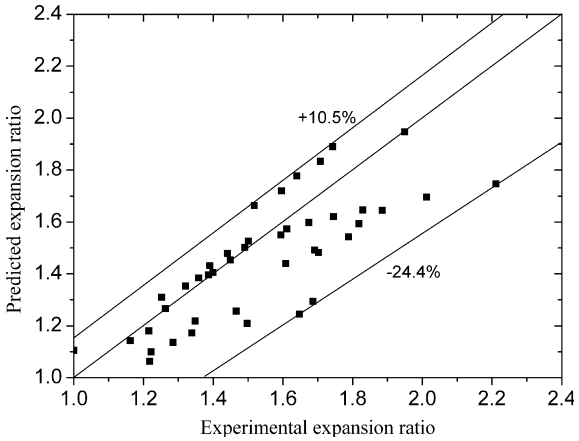

Fig. 6. Predicted expansion ratio compared with experimental expansion ratio.

Kim et al., 2001; Petrovic, 2005). There are two experimental methods to measure the penetration length: (1) analyzing the pictures obtained by the high speed video camera (2) measuring the temperature profiles along the nozzle axis. The accuracy of the first method is determined by the technology of taking pictures and image-analyzing, it is difficult to estimate the penetration length when the water temperature is high and the shape of steam plume becomes unstable. Although the exact penetration length measured by the second method may be obtained easier, it seems unreasonable for the great difference compared with the penetration length obtained by the first method. Furthermore, it is unfeasible when the temperature profile does not always decrease along the nozzle axis. In this work, the first method was adopted.

Figs. 7 and 8 show the dimensionless penetration length of steam plume (ratio between the length of steam plume and the inner diameter of nozzle exit) under two different nozzles. As the steam mass flux and water temperature increase, the dimensionless penetration length of steam plume increases, the values are in the range of 3.05–13.15.

As shown in Fig. 2, neglecting the effect of buoyant and assuming an axially symmetric flow, the dimensionless penetration length of steam plume L can be obtained according to the expression by Kerney et al. (1972) and Chun et al. (1996).

$$L = l/d_e = 0.5(G_e/G_m)^{1/2}/(S_m B) \tag{6}$$

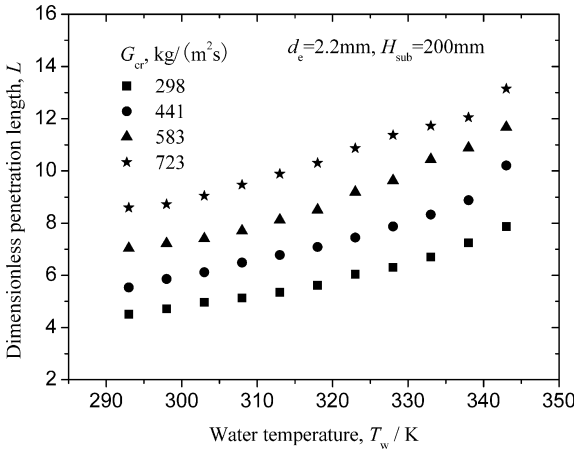

Fig. 7. Dimensionless penetration length of steam plume (Nozzle a).

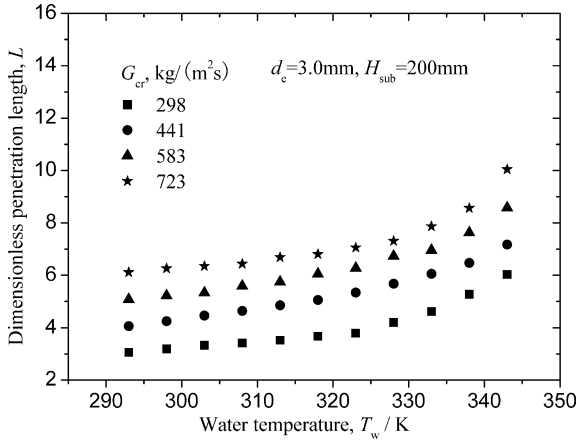

Fig. 8. Dimensionless penetration length of steam plume (Nozzle b).

where l is the penetration length of steam plume, d_e is the inner diameter of nozzle exit, G_e is the steam mass flux at nozzle exit, G_m is taken to be equal to the critical steam mass flux at ambient water pressure, $B = c_p\Delta T/h_{fg}$ is the condensation driving potential, c_p is the liquid special heat, ΔT is the temperature difference between both phases, h_{fg} is the releasing heat of condensation, S_m is the mean transport modulus which is assumed to be a constant according to the experimental data (Kerney et al., 1972).

When the water temperature increased, the errors of the predicted penetration length by Eq. (6) would increase due to the increasing uncertainty of the tip of steam plume. For the two nozzles, the predicted errors were within the band of 40%. According to the analysis, it indicated that the increase of the water temperature would lead to the overestimate of the predicted penetration length while the steam exit pressure has the analogous effect. Therefore, considering these factors and the effect of the nozzle structure parameters, a correctional correlation for the dimensionless penetration of steam plume could be given as

$$L = 0.868B^{-0.6}(p_s/p_a)^{0.2}(G_e/G_m)^{1/2} \tag{7}$$

where p_s, p_a are the pressure of inlet steam and pressure of ambient water, respectively.

Fig. 9 shows the predicted dimensionless penetration length by Eq. (7) and the correlations of Kerney et al. (1972); Chun et al. (1996) and Kim et al. (2001), respectively, which were compared with the experimental dimensionless penetration length. As shown in Fig. 9, it can be seen that the previous correlations given

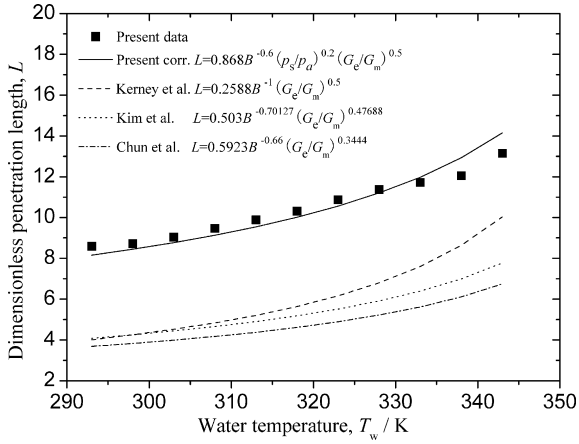

Fig. 9. Comparison of dimensionless penetration length with other correlations (nozzle a, $G_{cr} = 723$ kg/s).

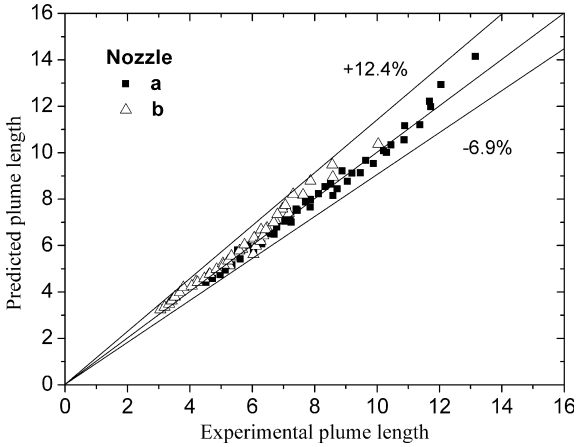

Fig. 10. Predicted penetration length compared with experimental penetration length.

for the sonic steam jet condensation are not suitable for the supersonic steam jet condensation. But the predicted penetration lengths by Eq. (7) are well in accord with the experimental penetration lengths.

In addition, the errors of the predicted penetration lengths by Eq. (7) compared with the experimental penetration lengths are shown in Fig. 10.

3.5. Condensation heat transfer coefficient

Although much research has been carried out on the direct contact condensation heat transfer, the exact heat transfer coefficient can not be obtained theoretically or experimentally due to the numerous interdependent parameters and the complexity of the corresponding physical mechanisms. In this work, the interfacial transfer model due to the shear stress (Kim et al., 2004) was adopted to predict the heat transfer coefficient. The condensation heat transfer coefficient was given by

$$h_{\mathrm{con}} = 0.14 G_{\mathrm{e}} \sqrt{\frac{k_l c_{\mathrm{p}}}{v_l \rho_{\mathrm{v}}} \frac{1}{4-2\delta} L^{-1}} \tag{8}$$

where k_l is the thermal conductivity of water, v_l is the kinematic viscosity of water, ρ_{v} is the density of vapor, δ is the steam plume shape factor which is defined as $\delta = \frac{l-x_{\mathrm{m}}}{l}$, x_{m} is the axial distance at maximum expansion ratio.

Then combining the Eqs. (7) and (8), the condensation heat transfer coefficient can be obtained as follows:

$$h_{\mathrm{con}} = 0.1503 \sqrt{\frac{k_l c_{\mathrm{p}}}{v_l \rho_{\mathrm{v}}} \frac{1}{4-2\delta}} G_{\mathrm{e}}^{0.75} G_{\mathrm{m}}^{0.25} B^{0.3} \left(\frac{p_{\mathrm{a}}}{p_{\mathrm{s}}}\right)^{0.1} \tag{9}$$

The predicted condensation heat transfer coefficients calculated by Eq. (9) are shown in Fig. 11. It indicates that the condensation heat transfer coefficient is in the range of 0.59–1.92 MW/m^{2}K.

According to Eq. (6) and the transport modulus $S = h/(c_{\mathrm{p}} G)$, the correlation $h_{\mathrm{ave}} = 0.5 C_{\mathrm{p}} G_{\mathrm{e}} B^{-1} L^{-1} (G_{\mathrm{e}}/G_{\mathrm{m}})^{1/2}$ can be obtained. Here, the predicted L by corrected Eq. (7) is used, so the average condensation heat transfer coefficient can be given as

$$h_{\mathrm{ave}} = 0.576 c_{\mathrm{p}} G_{\mathrm{e}} B^{-0.4} \left(\frac{p_{\mathrm{a}}}{p_{\mathrm{s}}}\right)^{0.2} \tag{10}$$

Fig. 12 shows the average condensation heat transfer coefficients under different water temperatures and nozzles. It indicates that the condensation heat transfer coefficient is in the range of 0.63–3.44 MW/m^{2}K. Moreover, the heat transfer coefficient of supersonic jet condensation has the same magnitude with that of previous

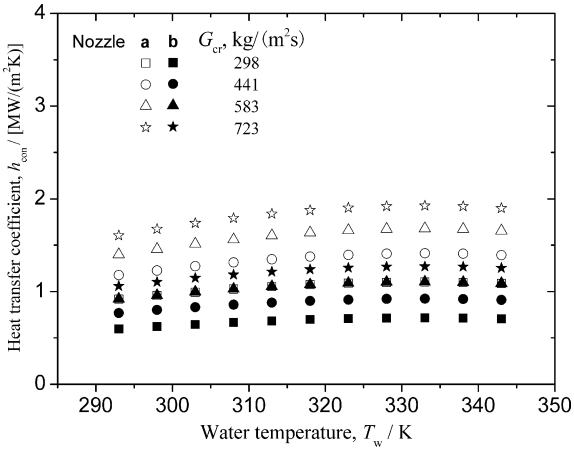

Fig. 11. Condensation heat transfer coefficient calculated by Eq. (9).

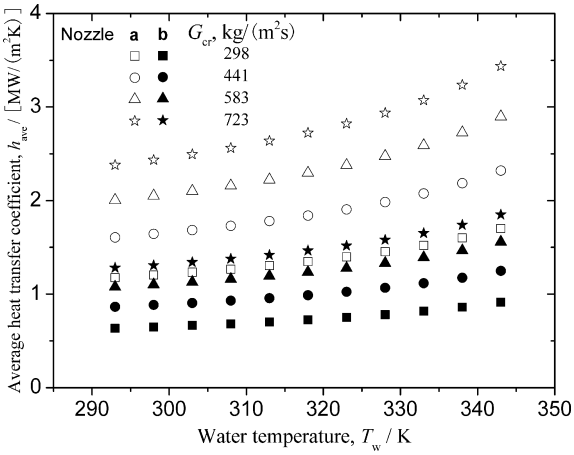

Fig. 12. Average condensation hear transfer coefficient calculated by Eq. (10).

sonic jet condensation, 1.00–3.50 MW/m^{2}K and 1.24–2.05 MW/m^{2}K given by Chun et al. (1996) and Kim et al. (2001), respectively.

As shown in Figs. 11 and 12, the heat transfer coefficients tend to increase as the steam mass flux increases and the diameter of nozzle exit decreases at the same test conditions. Although the effect of water temperature on the heat transfer coefficients is found to be smaller than that of steam mass flux and nozzle size, the heat transfer coefficients tend to increase slowly with water temperature in Fig. 12. But the heat transfer coefficient increases first then decreases with water temperature in Fig. 11. The possible reason for the two trends is given as follows. The heat transfer coefficient is determined by heat transfer temperature difference and heat transfer area. As the water temperature increases, the temperature difference between the two phases decrease, if the area changes little, the heat transfer coefficient would increase. Actually, the area is difficult to determine. Especially for high water temperature, the steam plume would become instable, but the turbulence between the two phases would increase. These factors may lead to a peak value of heat transfer coefficient in the range of testing water temperature. Therefore, the effect of water temperature on the steam jet condensation heat transfer is complicated, and the further study is needed to found the more precise model to predict the steam jet condensation phenomena.

4. Conclusions

The condensation of supersonic steam jet submerged in the quiescent subcooled water was investigated experimentally to find its characteristics and the difference compared with the previous sonic jet. The main results may be summarized as follows:

(1) Six different shapes of steam plume were found under the present test conditions, their distribution as a function of the steam exit pressures and water temperatures was found. The shape of steam plume was controlled mainly by the steam exit pressure and water temperature.
(2) As the increase of steam mass velocity and water temperature, the measured maximum expansion ratio and dimensionless penetration length of steam plume were in the ranges of 1.08–1.95 and 3.05–13.15, respectively.
(3) The average heat transfer coefficient of supersonic steam jet condensation was found to be in the range of 0.63–3.44 MW/m^2K. An analytical model of steam plume was set up and the correlations to predict the maximum expansion ratio, dimensionless penetration length and average heat transfer coefficient were also given.

Acknowledgements

This work was supported by National Natural Science Foundation of China (Nos. 50676078 and 50521604) and Program for New Century Excellent Talents in University of Chinese Education Ministry (NCET-04-0940).

References

Chan, C.K., Lee, C.K.B., 1982. A regime map for direct contact condensation. Int. J. Multiphase Flow 8, 11–20.
Chen, L.D., Faeth, G.M., 1982. Condensation of submerged vapor jets in subcooled liquids. Trans. ASME J. Heat Transfer 104, 774–780.
Chun, M.H., Kim, Y.S., Park, J.W., 1996. An investigation of direct condensation of steam jet in subcooled water. Int. Commun. Heat Mass Transfer 23, 947–958.
Currie, I.G., 2003. Fundamental Mechanics of Fluids, third ed. Marcel Dekker, Inc., New York.
Eden, T.J., Miller, T.F., Jacobs, H.R., 1998. The centerline pressure and cavity shape of horizontal plane choked vapor jets with low condensation potential. J. Heat Transfer 120, 999–1007.
Giovanni, D.T., Evasio, L., Mario, M., 1984. Experimental study on steam jet condensation in subcooled water pool. In: 3rd Multiphase Flow and Heat Transfer Symposium. Miami Beach, FL, USA. Part A, pp. 815–830.
Kazuyuki, Takase, Yasuo, Ose, Tomoaki, Kunugi, 2002. Numerical study on direct-contact condensation of vapor in cold water. Fusion Eng. Des., 421–428.
Kerney, P.J., Faeth, G.M., Olscn, D.R., 1972. Penetration characteristics of a submerged steam jet. AICHE J. 18, 548–553.
Kim, H.Y., Bae, Y.Y., Song, C.H., Park, J.K., Choi, S.M., 2001. Experimental study on stable steam condensation in a quenching tank. Int. J. Energy Res. 25, 239–252.
Kim, Y.S., Park, J.W., Song, C.H., 2004. Investigation of the steam-water direct contact condensation heat transfer coefficients using interfacial transport model. Int. Commun. Heat Mass Transfer 31, 397–408.
Kim, Y.S., Song, C.H., 2003. Overall review of steam jet condensation in a next generation reactor water pool. In: Proceedings of 2003 ASME International Mechanical Engineering Congress. November 15–21.
Kostyuk, V.I., 1985. The mechanism of the process of condensation of a jet of steam in a pool of liquid. Therm. Eng. 32, 34–37.
Liang, K.S., Griffith, P., 1994. Experimental and analytical study of direct contact condensation of steam in water. Nucl. Eng. Des. 147, 425–435.
Petrovic, A., 2005. Analytical study of flow regimes for direct contact condensation based on parametrical investigation. J. Press. Vess. Technol. 127, 20–25.
Sagar, S.G., Jyeshtharaj, B.J., Manish, S.S., Chaganti, S.R., Daya, S.S., 2006. CFD analysis of flow pattern and heat transfer in direct contact steam condensation. Chem. Eng. Sci. 61, 5204–5220.
Seong, H.J., Hee, C.N., Mayinger, F., 2000. Measurement of heat transfer coefficients for direct contact condensation in core makeup tanks using holographic interferometer. Nucl. Eng. Des. 199, 75–83.
Simpson, M.E., Chan, C.K., 1982. Hydrodynamics of a subsonic vapor jet in subcooled liquid. Trans. ASME J. Heat Transfer 104, 271–278.
Takeuchi, K., Cunningham, J.P., Haberstroh, R.C., 1994. Steam jet penetration into subcooled water in a vessel. In: International Mechanical Engineering Congress and Exposition, Chicago, NE-v15, pp. 19–28.
Weimer, J.C., Faeth, G.M., Olscn, D.R., 1973. Penetration of vapor jets submerged in subcooled liquids. AICHE J. 19, 552–558.
Youn, D.H., Ko, K.B., Lee, Y.Y., Kim, M.H., Bae, Y.Y., Park, J.K., 2003. The direct contact condensation of steam in a pool at low mass flux. J. Nucl. Sci. Technol. 40, 881–885.